We are IntechOpen, the world's leading publisher of Open Access books
Built by scientists, for scientists

6,900
Open access books available

185,000
International authors and editors

200M
Downloads

154
Countries delivered to

Our authors are among the

TOP 1%
most cited scientists

12.2%
Contributors from top 500 universities

CLARIVATE ANALYTICS
BOOK CITATION INDEX
INDEXED

WEB OF SCIENCE™

Selection of our books indexed in the Book Citation Index
in Web of Science™ Core Collection (BKCI)

Interested in publishing with us?
Contact book.department@intechopen.com

Numbers displayed above are based on latest data collected.
For more information visit www.intechopen.com

Homo- and Hetero-Covariance NMR Spectroscopy and Applications to Process Analytical Technology

Martin Jaeger and Robin Legner

Additional information is available at the end of the chapter

Abstract

Covariance processing of data and spectra has established itself among the computer-based NMR spectroscopy methodologies to increase sensitivity and resolution and to facilitate spectral analysis. While homo-correlations yield two-dimensional (2D) diagonally symmetric or antisymmetric spectra, hetero-covariance transformations allow to transfer NMR chemical shift information to other spectroscopic techniques, such as near infra-red or Raman. This is visualized as a 2D correlation map, provided a common indirect or perturbation domain, such as time, concentration change, and pressure. Covariance spectra can be generated as synchronous or asynchronous maps. The synchronous map relates the signals of species, e.g., educts and products. The asynchronous spectrum allows to derive the sequential order in which such species occur relative to each other. After a theoretical introduction into covariance NMR, its application in process analytical technology is discussed for wine fermentation, a radical polymerization reaction, a continuous process ethanol production using immobilized yeast, and a Knoevenagel condensation in a microreaction system. The covariance approach is extended toward two perturbation variables and quantitative relationships through PARAFAC kernel analysis and is illustrated for the preparation of polylactic acid nanocomposites. The advantages and added values of using synchronous and asynchronous spectra to gain process knowledge and control are demonstrated.

Keywords: homo- and hetero-correlation spectroscopy, covariance NMR, synchronous and asynchronous spectra, process analytical technology, Raman spectroscopy

1. Introduction

Striving for enhanced sensitivity, specificity, and resolution NMR spectroscopy traditionally turned to creating stronger magnets, thus higher magnetic field strengths. The implementation of pulsed-field gradients and the development of cryogenically cooled probes contributed

further to increasing instrumental sensitivity. In recent years, vivid interest was paid to so-called fast NMR methods for taking another step in ameliorating the signal-to-noise ratio. Fast methods followed several approaches. These consisted of pulse-sequence-based methods, such as time-shared experiments, hardware oriented strategies, such as parallel acquisition and detection, and the combination of two or more NMR experiments into one pulse sequence. They all aimed at optimization to take advantage of a given experimental timeframe. Not only the long-time used spectral acquisition schemes were re-evaluated, the spectral processing procedure was also equally subjected to re-investigation. As a consequence, the so-far untouched Fourier Transformation (FT), being at the heart of multi-dimensional NMR spectroscopy, was challenged. Statistic data treatment turned out to transform experimentally acquired data into spectra evenly well. Covariance transformations were applied to raw data sets as well as pre-processed data. Covariance NMR and covariance processing methods have been recently reviewed in great detail [1–7]. Due to the purely mathematical nature, the computer power and the algorithms applied determine the speed with which covariance spectra can be obtained. The experimentally acquired data determine the sensitivity observed in the covariance spectrum [8].

Beyond NMR, covariance transformations have been known to be of a very general nature according to Eq. (1) [9, 10]. The potential of generalized covariance processing was soon recognized, thus allowing traditional one-dimensional (1D) spectroscopic techniques such as infra-red (IR) and Raman spectroscopy to yield two-dimensional (2D) spectra [11, 12]. To fully exploit Eq. (1), data matrices of two distinct spectroscopic techniques, such as NMR and IR, were transformed to yield a two-dimensional IR-NMR spectrum, and the technique was baptized hetero-spectroscopy [13, 14]. As a prerequisite for its application, the spectra need to possess a common dimension prior to transformation, e.g., reaction time or change in sample pressure, called the perturbation dimension. The technique proved not only suitable for the transformation of heterogeneous data arrays or spectra but also helpful to visualize valuable information via correlation signals and their phases [12, 15]. Correlation signals indicated spectral constituents that share a common fate. The phases reflect simultaneous or asynchronous increase or decrease of the spectral constituents.

In this report, covariance NMR spectroscopy, in particular correlation and hetero-covariance NMR, shall be described in theory and practice for the investigation of chemical reactions and batch characterization. Illustrative examples shall be given how NMR spectroscopy can help attribute and distinguish signals from different spectroscopic techniques that provide lower spectral resolution or ambiguity for the assignment. In this respect, contributions of correlation spectroscopy, homo- and hetero-covariance NMR spectroscopy to the field of Process Analytical Technologies (PAT), shall be reported.

2. The concept of homo- and hetero-covariance spectroscopy

Covariance stems from statistical mathematics. Variances represent the deviation from the mean of a series of data. The covariance C in matrix form according to Eq. (1) is understood

as the difference between the correlated and the uncorrelated products of a series of data [9, 10, 16].

$$\mathbf{C}(x, y) = \langle (x - \langle x \rangle)(y - \langle y \rangle) \rangle = \langle xy \rangle - \langle x \rangle \langle y \rangle \tag{1}$$

where $\langle x \rangle$ and $\langle y \rangle$ are the mean values, and $\langle \ \rangle$ represents any type of correlation function.

Let x and y in Eq. (1) be spectroscopic data series and be arranged such that S represents a spectrum of N_1 data points, and the elements C_{ij} of the covariance matrix or covariance map $\mathbf{C}$ are calculated in Eq. (2) as follows:

$$C_{ij} = \frac{1}{N_1 - 1} \sum_{k=1}^{N_1} \Big(S(k, i) - \langle S(i) \rangle \Big) \Big(S(k, j) - \langle S(j) \rangle \Big) \tag{2}$$

$$\langle S(i) \rangle = \frac{1}{N_1} \sum_{k=1}^{N_1} S(k, i) \tag{3}$$

where the average spectrum is defined as $\langle S(i) \rangle$ in Eq. (3). Substitution of i by j defines $\langle S(j) \rangle$ analogously. In mathematical contexts, Eqs. (1) and (2) are common. For spectroscopy, the symbols for time and frequency, t and v or ω, are more often used. Applying Parseval's theorem (4) to Eqs. (1) and (2), the covariance matrix can be expressed by Eq. (5).

$$\int_{-\infty}^{\infty} f(t) g^*(t) dt = \frac{1}{2\pi} \int_{-\infty}^{\infty} F(\omega) G^*(\omega) d\omega \tag{4}$$

The two data sets denoted either s, S, Φ, or Ψ in Eq. (5) consist of mixed time-frequency data before and frequency-frequency data after transformation. They also share a common indirect dimension. The latter can be interpreted in terms of a perturbation, and the dimension is hence called perturbation dimension [9].

$$\begin{aligned} C(\omega_{2,A}, \omega_{2,B}) &= \langle s(t_{inc}, \omega_{2,A}) \cdot s(t_{inc}, \omega_{2,B}) \rangle \\ &= \frac{1}{2\pi(T_{max} - T_{min})} \int_{-\infty}^{\infty} S(\omega_{inc}, \omega_{2,A}) \cdot S^*(\omega_{inc}, \omega_{2,B}) d\omega_{inc} \\ &= \Phi(\omega_{2,A}, \omega_{2,B}) + i\Psi(\omega_{2,A}, \omega_{2,B}) \end{aligned} \tag{5}$$

The index inc refers to the second or indirect spectral dimension. In a typical experiment, this dimension is recorded as discrete time intervals between a maximum limit T_{max} and a minimum limit T_{min}. The direct dimension may stem from two different data sets, $A \neq B$, or from the same data set, $A = B$. In the latter case, the data sets are transposed with respect to each other.

The spectra or maps Φ and Ψ are defined according to Eqs. (6) and (7).

$$\Phi(\omega_{2,A}, \omega_{2,B}) = \frac{1}{T_{max} - T_{min}} \int_{T_{max}}^{T_{min}} s(t_{inc}, \omega_{2,A}) \cdot s(t_{inc}, \omega_{2,B}) dt_{inc} \tag{6}$$

$$\Psi(\omega_{2,A}, \omega_{2,B}) = \frac{1}{T_{max} - T_{min}} \int_{T_{max}}^{T_{min}} s(t_{inc}, \omega_{2,A}) \cdot h \cdot s(t_{inc}, \omega_{2,B}) dt_{inc} \tag{7}$$

where h is the Noda-Hilbert transform [15]. The reader is also referred to Eqs. (17) and (18) for definition and matrix notation. Integration of Eqs. (6) and (7) results in Eqs. (8) and (9).

$$\Phi(\omega_{2,A}, \omega_{2,B}) = p(\cos\varphi)^{A,B} Abs(\omega_{2,A}) Abs(\omega_{2,B}) \tag{8}$$

$$\Psi(\omega_{2,A}, \omega_{2,B}) = q(\sin\varphi)^{A,B} Abs(\omega_{2,A}) Abs(\omega_{2,B}) \tag{9}$$

Equations (8) and (9) are lengthy expressions when fully written for p and q. Yet, the phase φ is readily recognized. It may be considered as an internal reference according to Eqs. (10) and (11), which present the important parts of the complete definition for p and q.

$$p(\cos\varphi)^{A,B} \sim \cos(\omega_{2,\alpha}t_{inc} + \varphi), \ \alpha = A, B \tag{10}$$

$$q(\sin\varphi)^{A,B} \sim \sin(\omega_{2,\alpha}t_{inc} + \varphi), \ \alpha = A, B \tag{11}$$

The comparison of Eqs. (11) and (12), the latter being an analogous expression but obtained after Fourier Transformation, readily reveals that an internal reference φ is absent in Eq. (12), i.e., manual phase correction after FT is required in contrast to the covariance transformed version of the spectral representation.

$$S(\omega_{inc}, \omega_2) = \int s(\omega_{inc}, \omega_2) \exp(-i\omega_2 t_{inc}) dt_{inc}$$

$$= \int s(t_{inc}, \omega_2) \cos(\omega_{inc}, t_{inc}) dt_{inc} \tag{12}$$

$$+ i \int s(t_{inc}, \omega_2) \sin(\omega_{inc}, t_{inc}) dt_{inc}$$

A spectrum after FT often consists of the real part data, with the imaginary part discarded. Yet, the phase still needs to be adjusted. The interested reader is referred to NMR textbooks and to the recent works in the context of covariance NMR [17, 18].

Equation (13) is the general form of Eq. (3). Here, f and ω denote spectral variables, such as frequencies, that may be recorded using any type of spectroscopy. A common perturbation such as a time domain t relates them to each other. Nevertheless, the perturbation could also be a series of samples, pressure, crystallization, etc.

$$C(f, \omega) = \langle s_1(f, t) \cdot s_2(\omega, t) \rangle \tag{13}$$

Spectra generated using Eq. (13) represent hetero-spectral correlation maps [14]. For pure NMR spectroscopy, unsymmetrical indirect covariance NMR was the first type of hetero-correlation spectroscopy, relating, e.g., ^{15}N and ^{13}C signals via the proton dimension, to each other [19–21]. Taken a step further, NMR and IR or NMR and mass spectrometry data were correlated to each other [22].

The covariance matrix contains as its elements the covariance C_{ij}, i.e., the amplitudes of positions i and j of the 1D spectra. Rewriting Eq. (2) in matrix form yields the relationship

between C and the spectroscopic data set S. The matrix multiplication of S with its transpose S^T is equal to C^2, cf. Eq. (14).

$$C^2 = S^T \cdot S \tag{14}$$

The complete mathematical derivation and proofs have been accomplished by Brüschweiler et al. and Noda et al. [16, 23, 24].

Defining S as the mixed time-frequency matrix, $S(t_1, \omega_2)$, the product $S^T S$ is the symmetric matrix $C(\omega_1, \omega_2)$. A common two-dimensional NMR spectroscopic data set S often has $N_1 = 2\,k$ and $N_2 = 256\,k$ data points. Hence, the resulting covariance map will be of dimensions $N_1 \times N_2 = 2\,k \times 2\,k$. This has been assumed as a projection of the direct or acquisition dimension onto the indirect or incremented dimension. It is readily recognized that the indirect dimension is thus substantially enlarged. Two data matrices F^T and F that have been the results of two-dimensional Fourier transformation may also be multiplied to form the covariance spectrum according to Eq. (15).

$$C^2 = S^T \cdot S = F^T \cdot F \tag{15}$$

The equality of transformations of the mixed time-frequency data and the completely Fourier transformed data is a consequence of Parseval's theorem (4) and ensures that the transformations of the mixed time-frequency data and the Fourier transformed data are equal [16, 24]. From another perspective, the spectral reconstruction can be considered as relating two direct dimensions through an indirect dimension or perturbation, which is discarded. The physical meaning of the indirect dimension is therefore of little importance. Thus, it relates Noda's model two IR wavenumber dimensions via a common perturbation, which may be time, pressure, temperature, sample space, or many more [13]. The matrix representation form reveals that Noda's synchronous matrix Φ, in Eqs. (6) and (16), corresponds to the covariance map according to Eq. (15), if mean centered spectra are the elements of the data matrices giving Φ. The asynchronous map Ψ of Eqs. (7) and (17) corresponds to the indirect covariance correlation spectrum. Equations (15) and (13) further extend covariance spectroscopy to hetero-correlation spectroscopy.

Eqs. (16) and (17) finally represent the matrix notation of equations as the synchronous map or spectrum and as the asynchronous map.

$$\Phi = \overline{X}^T \cdot \overline{X} \tag{16}$$

$$\Psi = \overline{X}^T \cdot N \cdot \overline{X} \tag{17}$$

where $\overline{X}$ is the matrix of mean-centered spectra and N the Noda-Hilbert orthogonalization matrix with $N_{ik} = 0$ if $i = k$ and $1/(\pi(k - i))$ otherwise.

Synchronous and asynchronous maps or spectra have some particular features [11]. Since synchronous homo-correlation spectra are computed from a data matrix and its transposed matrix, they are symmetric. They exhibit diagonal peaks, also called autopeaks, that are the

autocorrelation functions of spectral intensity variations. They hence reflect the amount of change the corresponding signal experiences along the perturbation dimension. Off-diagonal signals correlate two signals changing simultaneously or coincidently under the influence of the perturbation. When both signals increase or decrease, the sign of the crosspeak is equal to that of the diagonal peaks. If they behave adversely, the sign is opposite. It is readily recognized that the resolution of spectra can be enhanced by the spread into two dimensions. Furthermore, the occurrence of two or more components, such as educt and product, can be readily seen and facilitate signal assignments. An example for a synchronous spectrum is given in **Figure 1(a)**. As will be shown below, synchronous spectra are useful in homo- and hetero-covariance NMR spectroscopy.

The asynchronous spectrum in general is less easily interpreted. As a consequence of the Noda-Hilbert orthogonalization, cf. Eq. (17), no diagonal peaks are observed. The spectrum visualizes successive or sequential changes of signal intensities, which forbids the occurrence of autopeaks. The asynchronous map is antisymmetric with respect to the diagonal. Noda has shown that $\mathbf{\Psi}(\omega_i, \omega_j) = -\mathbf{\Psi}(\omega_j, \omega_i)$. [11]. The sign of a crosspeak is positive—positive is defined as in phase with the diagonal peak in the corresponding synchronous spectrum—if the intensity in dimension 1 changes predominantly before that in dimension 2 in the sequence of the perturbation. This is valid for crosspeaks above the diagonal, i.e., $\omega_1 > \omega_2$. A negative crosspeak is obtained when the order is reversed. An illustration is given in **Figure 1(b)**. Specie B of the example hence occurs before A, and C before D. Thorough derivations and discussions have been accomplished previously [11].

Despite its ability to correlate non-simultaneous occurrence of signals, the asynchronous map does not allow the analysis of population dynamics as in a two-step chemical reaction. As a
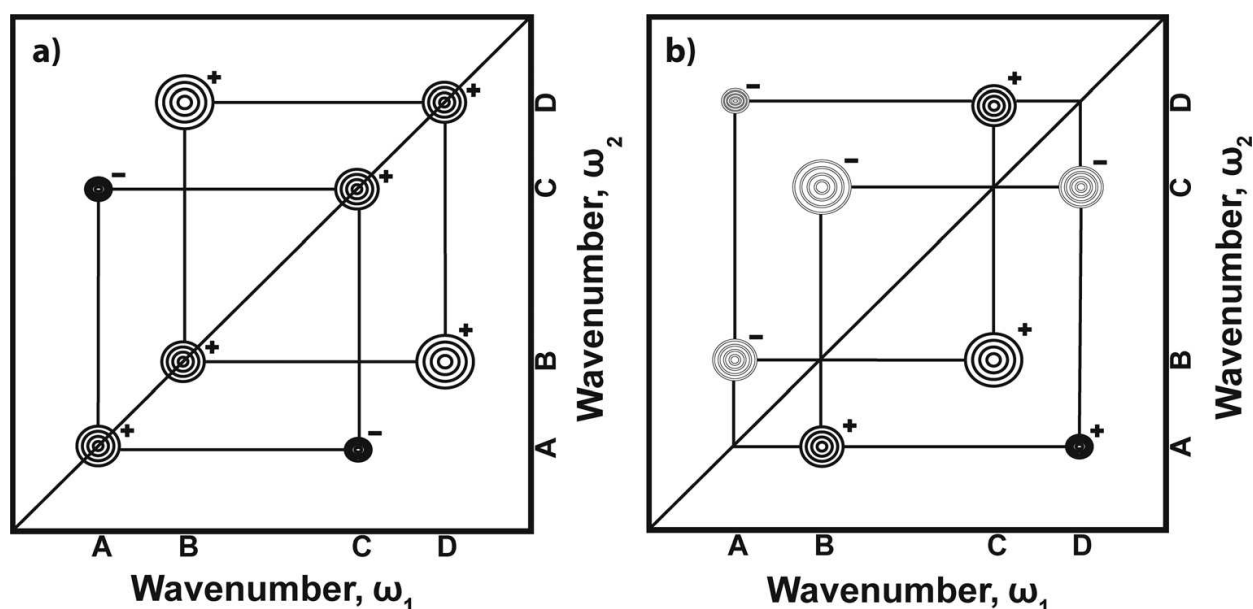

Figure 1. Schematic contour map of synchronous (a) and asynchronous (b) 2D correlation spectra. Peaks located at the diagonal are autopeaks. The signs of the correlation peaks are indicated. The intensity changes and signs are interpreted according to Noda's rules [11].

remedy to this problem, Noda devised two-dimensional codistribution spectroscopy [25]. Here, a moment analysis of spectral intensity distribution over the perturbation dimension was included, which accounted for the sequential attribution of species within a model chemical reaction A→B→C.

Out of the manifold of variations to combine raw and Fourier transformed data, a variety of covariance-transformed spectral representations have been introduced and their applications have been demonstrated: Among those used in NMR spectroscopy, the most often used or described were direct covariance, indirect covariance, doubly indirect covariance, unsymmetrical indirect covariance, generalized indirect covariance, which replaced the previous one, multidimensional covariance in form of Triple-Rank Covariance and 4D Covariance [2, 26–29]. Furthermore, the family of Statistical Correlation Spectroscopy (STOCSY) has been introduced, and its usefulness is demonstrated in many applications [22, 30–32].

For other spectroscopic techniques or combinations thereof, covariance spectroscopy is often referred to as 2D correlation spectroscopy, and hetero-covariance spectroscopy is called hetero-spectral, hetero-perturbation, and hetero-sample correlation spectroscopy [33]. Noda has further coined the term multiple perturbation 2D correlation, where the use of the parallel factor (PARAFAC) kernel analysis may play a key role in future spectral analysis [34–36]. As another variant, orthogonal sample design (OSD) was introduced and applied [37–39].

Multiple perturbation 2D correlation spectroscopy has been introduced recently by Shinzawa et al. [40, 41]. It is based on the extension of Eq. (3) yielding Eqs. (18) and (19) as follows:

$$\langle S_p(\omega, q)\rangle = \frac{1}{P}\sum\nolimits_{p=1}^{P} S(\omega, p, q) \tag{18}$$

$$\tilde{S}(\omega, p, q) = S(\omega, p, q) - \langle S_p(\omega, q)\rangle \tag{19}$$

where S is a set of spectra depending on frequency ω exposed to multiple perturbations $p = 1,2,…P$ and $q = 1,2,…Q$, such as time, temperature, concentration, etc. $\langle\ \rangle$ denote the average spectrum. Partial synchronous and asynchronous correlation spectra are computed according to Eqs. (20) and (21) in analogy to Eqs. (6) and (7).

$$\Phi_p(\omega_1, \omega_2, q) = \frac{1}{P-1}\sum\nolimits_{p=1}^{p} \tilde{S}_p(\omega_1, p, q) \cdot \tilde{S}_p(\omega_2, p, q) \tag{20}$$

$$\Psi_p(\omega_1, \omega_2, q) = \frac{1}{P-1}\sum\nolimits_{p=1}^{P} \tilde{S}_p(\omega_1, p, q) \cdot \tilde{S}_p^{\neq}(\omega_2, p, q) \tag{21}$$

where $\tilde{S}_p^{\neq}$ denotes the Hilbert-Noda transformation in this case given by Eq. (22).

$$\tilde{S}_p^{\neq}(\omega_2, p, q) = \sum\nolimits_{r=1}^{P} N_{pr}\tilde{S}_p(\omega_2, r, q) \tag{22}$$

with $N_{pr} = 0$ for $p = r$ and $N_{pr} = 1/((r - p)\pi)$ otherwise.

The PARAFAC kernel decomposes the data into scores and loading vectors. The original three-way data array is rearranged into a two-way data array by means of the so-called Kathri-Rao

($|\otimes|$) product, which implies the use of the Kronecker product $\otimes$. The matrix decomposition is usually achieved through solving an alternating least-squares problem iteratively. Disregarding the matrix of the residuals for the minimization problem, Eq. (23) is the fundamental matrix representation of the multiple perturbation correlation analysis.

$$X = A(C| \otimes |B)^T \qquad (23)$$

where X contains spectral data, A and C refer to perturbations 1 and 2, and B contains the spectral variable. The p-synchronous and p-asynchronous kernel matrices are similar to their analogs in Eqs. (16) and (17) but formed mean-centered and normalized score-vector matrix A. The ij-element of the p-synchronous kernel matrix as well as of the asynchronous one assumes values between -1 and $+1$, giving a similarity measure in the synchronous case and a dissimilarity measure in the asynchronous case between the score vectors of the ith and jth components. Evenly comparable, the sequential order of signal changes can be derived from the signs of the kernel matrix elements. The signal of the ith species changes before that of the jth when the signs of the ij-elements of the synchronous and asynchronous kernel matrix are the same. The order is reverted if the elements possess opposite signs. Spectral analysis can be carried out as well by performing the computation with the score matrix C instead of A. Complete mathematical descriptions have been published by Shinzawa et al. [34, 41].

Software suitable for covariance processing has recently been reviewed as well [3, 42]. With respect to some of the work performed in this report, we would like to direct the reader's attention to 2DShige. While this program is not especially dedicated to NMR spectroscopy, it is capable of performing hetero-spectroscopic covariance transformations. The program was devised by Morita and may be accessed for download via https://sites.google.com/site/shigemorita/home/2dshige. Covariance transformations applied therein follow the work by Noda. Synchronous and asynchronous maps are computed from data in CSV format.

The following section will focus on Process Analytical Technology (PAT) such that the stage will be set for the applications of covariance processing and NMR spectroscopy to process monitoring or process understanding.

3. A brief outline of process analytical technologies and microreaction processes

Process analytical technologies (PAT) have grown into an integral part of industrial manufacturing processes. The development of a process on a laboratory scale, the collection of data as well as monitoring of the production process in place are directed toward a well-understood process to ensure final product quality [43, 44].

This knowledge first enables process control and then process improvement. The envisaged process optimization is aimed at cost reduction, sustainability, and safety. Generally, production processes proceed on a large scale. The analytical instruments used close to the process are robust, relatively easy to operate instruments. Only for the development or validation of the analytical method are the dimensions of such large-scale processes reduced to laboratory

scales. The analytical instruments yet may be of the same size but more complex and of higher sensitivity and resolution.

Process analytical technologies often make use of spectroscopic and chromatographic as well as of integral methods. Today, Raman spectroscopy and near IR (NIR) spectroscopy play major roles, whereas pH, pressure, and refractivity techniques are typical non-specific methods, inexpensive still ubiquitous, and powerful within well-controlled processes [45]. The conditions of the production process often demand for greater robustness, stability, and performance of the analytical instruments, because of the close proximity to the manufacturing line. Process monitoring and control require prompt or real-time data recording, processing, and feeding the data back to the process control unit. These constraints necessitate in-line, on-line, or at least at-line analytical methods [46].

Microprocesses or microreactions are conducted in very small-scale reactors and mixing devices equipped with tubing, pumps, and valves. The reaction set-up is composed in a Lego-like manner, cf. **Figure 2**. Microdevices allow for a highly efficient heat transfer as compared to
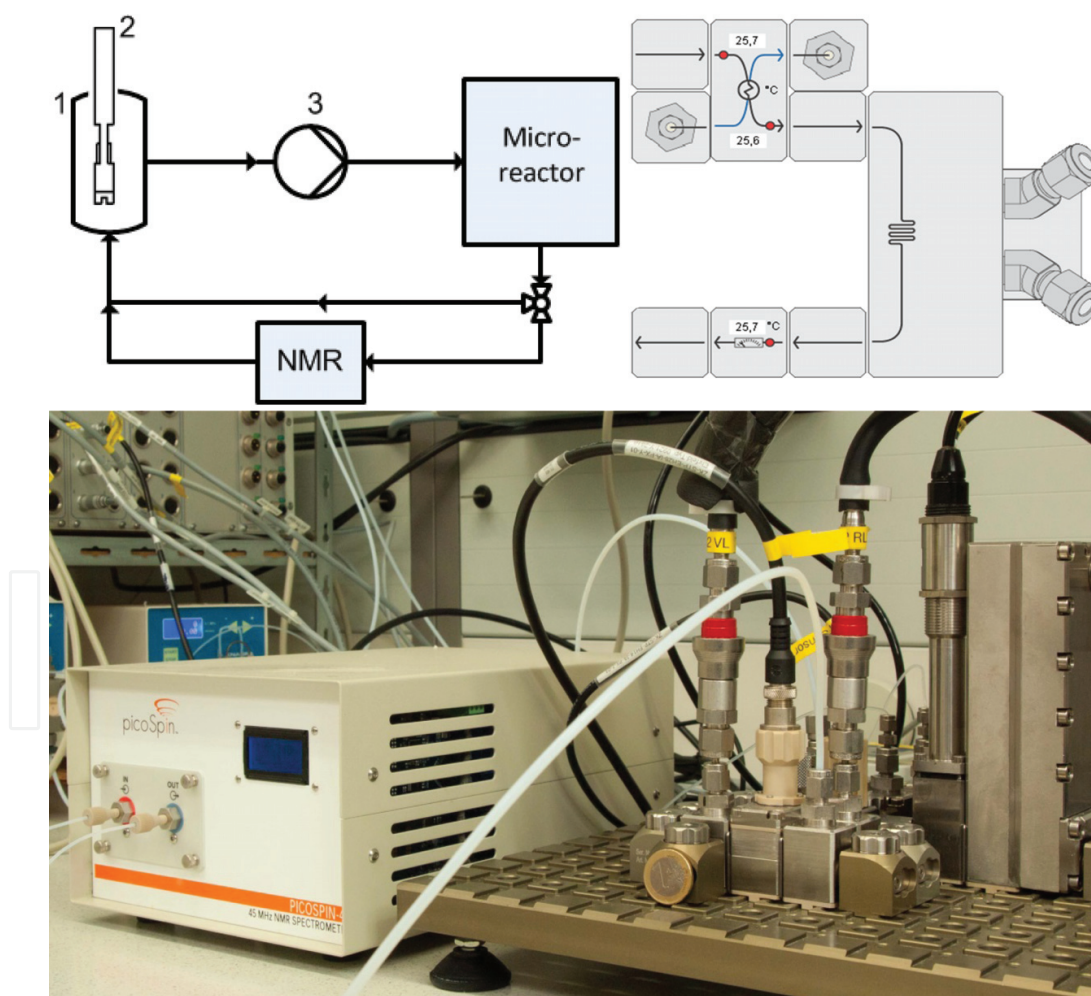

Figure 2. Microreaction assembly with on-line low-field ^{1}H-NMR spectrometer (bottom); process flow chart of the set-up of the microprocess analytics (top left): (1) storage vessel, (2) transflectance NIR immersion probe, (3) pump; zoom of the microreactor assembly (top right).

large-scale vessels. While they sometimes enable a superior mass transfer, they sometimes cause an inferior mixing of the reactants due to microfluidic effects. Typical yields may range from milligrams to a few grams per day depending on the reaction conducted in batch or flow mode [47–49].

Microprocesses with respect to scale, volumetric flow, and yield demand for microanalytics if implemented in-line or on-line. At-line installations merely require a sample cell of suitable size and sensitivity. Two different ways have been described to monitor microprocesses in-line or on-line with spectroscopic methods. The probes or sample cells were located either in the reaction vessel or a by-pass similar to large-scale facilities. Alternatively, the reaction was conducted within the sample cell of a spectrometer, e.g., UV/Vis or Nuclear Magnetic Resonance. Miniaturized analytical devices are preferable in case of microreaction vessels, whereas standard laboratory instruments may be used for the second case. So-called bench-top instruments are particularly interesting for microprocess analytical technology. Bench-top instruments may be found as the size of a microwave oven [50–53].

In the following sections, illustrative examples for the application of NMR spectroscopy, covariance, homo- and hetero-correlation spectroscopy to process monitoring, and process understanding will be given.

4. Applications of homo- and hetero-covariance spectroscopy

Covariance transformations of NMR data with or without prior Fourier transformation today are widely applied. Prominent examples comprise generalized indirect covariance and multidimensional covariance NMR as well as the combination of covariance and non-uniform sampling of data [54–57]. While the concept of homo- and hetero-covariance spectroscopy was developed nearly three decades ago, there are relatively few reports on the use of synchronous and asynchronous spectra involving NMR spectroscopy [3, 14, 55, 58, 59]. In contrast, an abundant number of investigations have applied so-called statistical hetero-spectroscopy (STOCSY) that has delivered important contributions to the field of metabolomics and whose variants have recently been depicted like a phylogenetic tree [22, 32, 60]. In the current report, the focus is however laid on examples from chemical processes rather than metabolomics.

4.1. Reaction monitoring of a wine fermentation

Kirwan et al. monitored a wine fermentation by ^{1}H NMR spectroscopy, drawing samples daily [61]. After careful preprocessing by segmentation, alignment, normalization, and smoothing, the data were covariance transformed, yielding homo-spectral synchronous and asynchronous matrices. While the synchronous map was found less prone to small chemical shift and linewidth variations, the asynchronous matrix was very sensitive. Sasic had also reported on the effects of linewidth [62]. In his metabonomics study on vasculitis analyzing rat urine samples, butterfly-like signal shapes were observed as a result of shifting peak positions. The lack of uniform pre-processing led to numerous artifacts and problems that severely hampered spectral interpretation in contrast to the wine study. The spectra recorded

in the wine fermentation study were hence ameliorated in a successive approach by imposing a fixed linewidth prior to covariance transformation such that the effects of linewidths changing during the fermentation were compensated for [63]. Extracted regions of both spectra are shown in **Figure 3**.

The spectra contained strong signals from sugars, fructose, and glucose, in the early period. In the later phase, ethanol signals became predominant. Other molecular species were emerging and vanishing as well. Their temporal relationship was said difficult to assess, which can be seen from inspection of **Figure 3**. A manifold of correlations are present in the covariance maps. Most clearly, the interdependence of the sugar and ethanol signals is recognized. Kirwan et al. already pointed out the difficulty of interpreting the spectra due to the high resolution of the initial ^{1}H NMR spectra leading to the large number of signals and correlations [61]. The authors suggested the use of slices through the synchronous map allowing the signal attribution and further extraction of the sequential information out of the corresponding slices of the asynchronous map. Careful analysis revealed that glucose was consumed and transformed at a higher rate than fructose, which was interpreted in terms of the different diffusion rates of the two sugars across the fermenting yeast cell membrane. The authors thus demonstrated the usefulness of correlation NMR spectroscopy for monitoring concentrations and sequential relationships in a biochemical process.

4.2. IR-NMR hetero-covariance spectroscopy applied to radical polymerization

Ryu et al. used 2D IR-NMR hetero-spectroscopy to characterize a chain transfer reaction during the radical polymerization of N-vinylpyrrolidone (NVP) [64]. Polyvinylpyrrolidone (PVP) was polymerized to form nanoparticles through a chain transfer reaction initiated by silver nitrate. Upon reduction via electron transfer, PVP polymer silver nanoparticles were
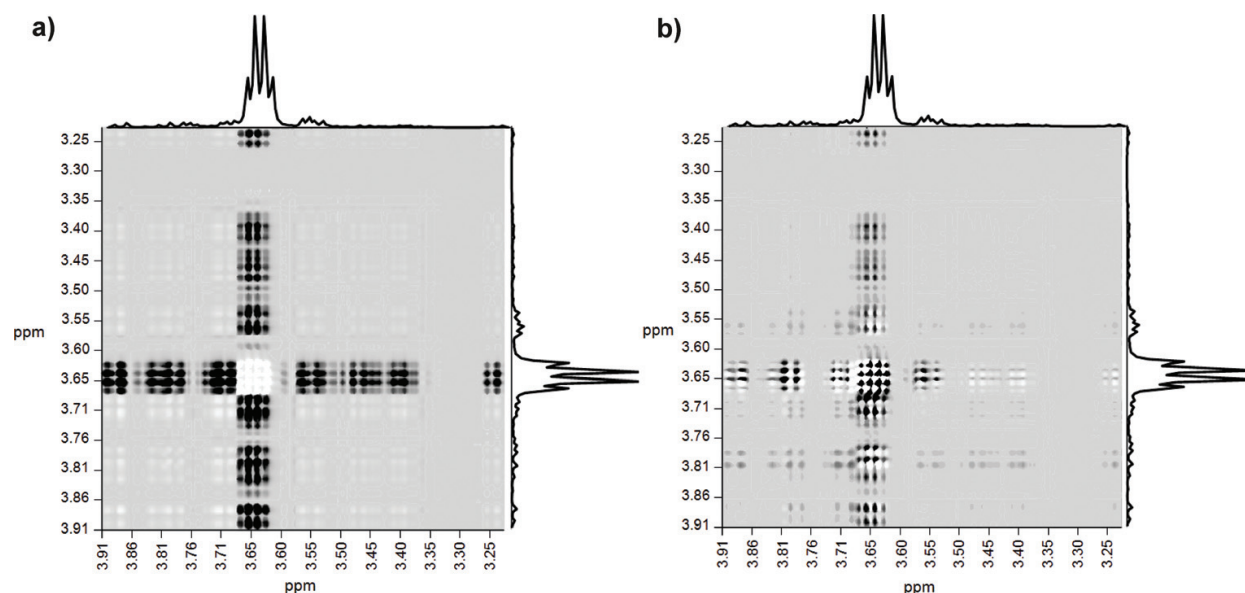

Figure 3. The synchronous (a) and asynchronous (b) maps of a section of the mean-centered 1D ^{1}H NMR spectra at 500 MHz of a series of wine fermentation samples. Reprinted from Kirwan et al. [63]. Copyright 2008, with permission from Elsevier.

formed. The resulting nanoparticles possessed a carbon-carbon double bond at the end of the PVP chain after chain transfer termination. Radical formation was initiated through azobisisobutyronitrile. The reaction was monitored using IR and 1D ^{1}H NMR spectroscopy. That is, a series of IR and NMR spectra depending on reaction time as perturbation domain were obtained. In the IR synchronous homo-correlation spectrum, bands at 1660 and 1676 cm^{-1} were revealed that could be attributed to the stretching vibration of the carbon-carbon double bond and of the carbonyl group, respectively. The asynchronous map was interpreted in terms of an intensity decrease of the band at 1660 cm^{-1} preceding the increase of the carbonyl band at 1676 cm^{-1}, cf. **Figure 4**.

Following Noda's rules on analyzing the synchronous and asynchronous spectral matrices, one might also come to a reversed conclusion concerning the sequential order [11, 12]. Both educt and product after chain transfer termination do exhibit carbon-carbon double bonds, where the NMR signals of the monomeric educts should lead to more intense signals due to less relaxation broadening. Yet, IR-NMR hetero-spectral correlation maps were used to unequivocally attribute the less-resolved IR bands in the product to the carbon-carbon double
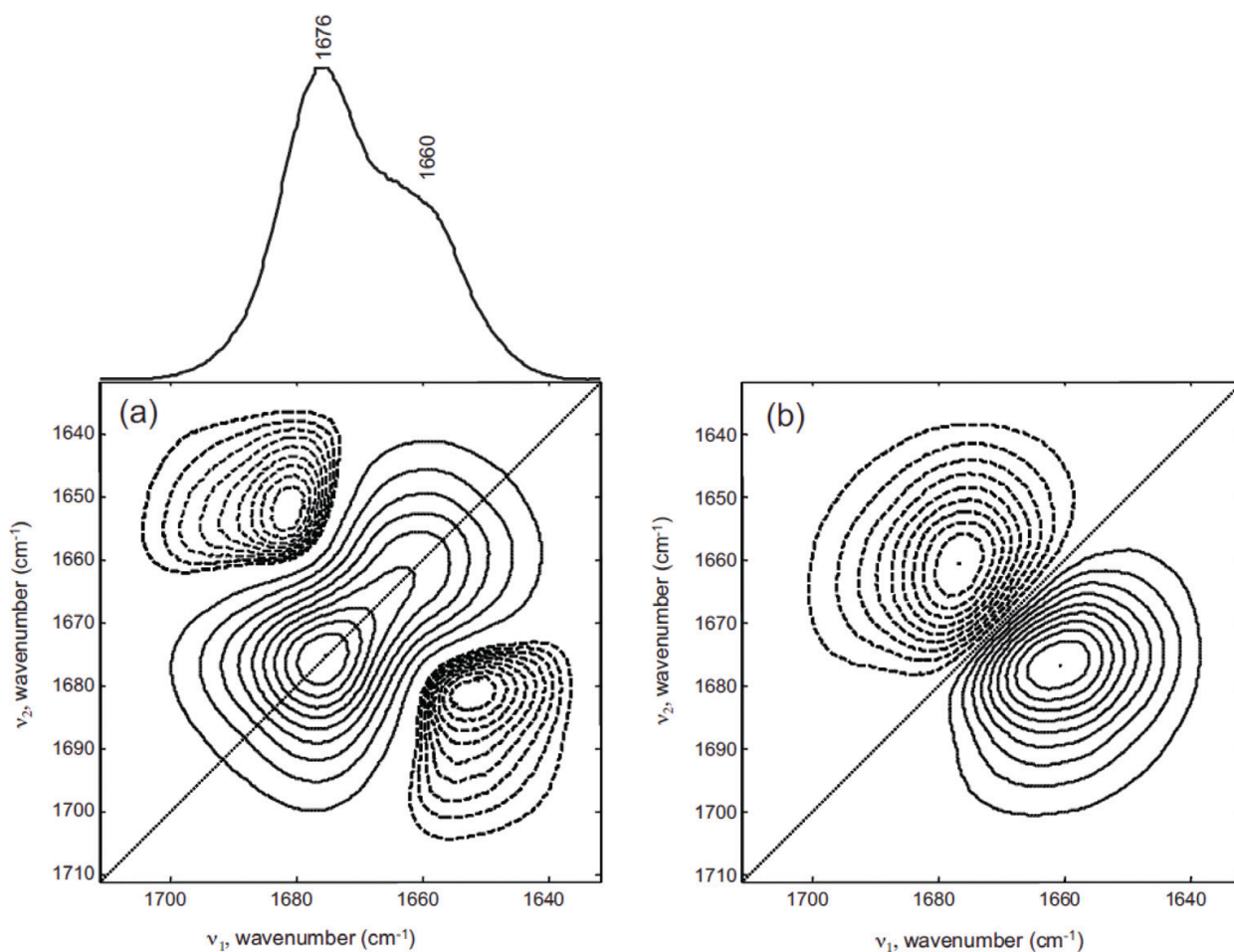

Figure 4. Synchronous (a) and asynchronous (b) 2D FTIR correlation spectra of PVP during polymerization with 400 ppm silver nitrate. The autopower spectrum extracted along the diagonal line in the synchronous 2D correlation spectrum is given on the top of (a). The solid and dashed lines in the spectra represent the positive and negative crosspeaks, respectively. Reprinted from Ryu et al. [64]. Copyright 2012, with permission from Elsevier.

bond and to the carbonyl group. Thus, both homo- and hetero-spectral correlations are of considerable value to increase spectral resolution and cross-fertilize the spectral analysis or assignment of one spectroscopic technique by taking advantage of another technique. This is especially helpful in process analytical technologies when signal crowding or strong overlap due to conditions unfavorable for a certain spectroscopic method occurs frequently.

4.3. Study of polylactic acid nanocomposites at varied temperatures and compositions using PARAFAC kernel analysis

Shinzawa et al. investigated polylactic acid nanocomposites using solid-state cross-polarization magic angle spinning (CP-MAS) ^{13}C NMR experiments [34]. They prepared four samples with varying clay content through a melt-blend process to obtain pellets. The properties of the sample exposed to temperature variation were studied by thermomechanical analysis. The elongation of the sample measured under imposture of a load occurred most notably at the glass transition temperature of the samples around 60°C. After a certain increase, a plateau was reached. The finding was interpreted that the plastic deformation observed was related to the glass-to-rubber transition of the amorphous polylactic acid component. When the elongation did no longer increase, a network structure due to physical crosslinkage induced by the crystalline domain was assumed. The dependence on the clay content suggested that with increasing clay inclusion, the tendency to elongate with temperature decreases. Thus, inclusion of clay led to enhanced stiffness. By applying NMR spectroscopy, Shinzawa et al. strove to probe the macroscopic properties on a molecular scale. To this purpose, they inspected the ^{13}C NMR resonance around 170 ppm, which originates from two peaks at 169 ppm and 170 ppm attributed to the crystalline and amorphous phases, respectively. Since NMR spectra depended on two separate perturbations, i.e., clay content and temperature, the PARAFAC kernel analysis according to Eq. (23) was employed for a detailed analysis. As described above, two sets of synchronous and asynchronous correlation spectra were obtained after the covariance transformations and matrix decompositions: the temperature-dependent and the clay-dependent homo-correlations. The partial correlations from composition-dependent NMR spectra at fixed temperature are exemplarily presented in **Figure 5**. Whereas the partial temperature-dependent correlation spectra revealed
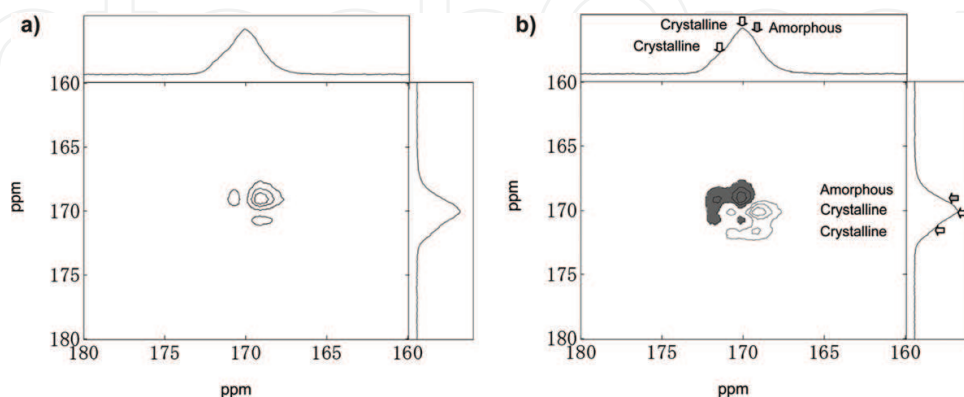

Figure 5. Partial synchronous correlation (a) and partial asynchronous correlation (b) spectra calculated from clay weight-dependent 1D CP-MAS ^{13}C NMR spectra recorded at 100.56 MHz. Reproduced from Shinzawa et al. [34] with permission of The Royal Society of Chemistry (RSC).

that the amorphous preceded the crystalline component upon temperature increase, the spectra in **Figure 5** showed that the amorphous content occurred predominantly before the crystalline content on increasing clay content. This was assumed due to the clay acting as a nucleating agent. It would foster additional crystallization of the polylactic acid. Upon decrease of the amorphous phase, the phase transitioning from glass to rubber should be reduced. These results were supported by the thermomechanical analysis.

The added value of the PARAFAC kernel analysis is that it furnishes quantitative data. The score, A and C, and loading, B, matrices reflect the change in signal intensity separated into composition and temperature dependence. They also provide abstract information on the dynamic behaviors of the crystalline and amorphous phases. The synchronous and asynchronous pair of the kernel matrix is exemplarily presented in **Figure 6** for the spectral intensity change of the nanocomposite samples due to clay content variation. The so-called q-synchronous correlation intensity, cf. above, $H_{q\ amorphous,\ crystalline} = -0.98$ and q-asynchronous correlation intensity $K_{q\ amorphous,\ crystalline} = 0.06$ were interpreted in terms of similarity of changes in the amorphous and crystalline components due to the presence of clay. Yet, the negative sign indicated opposite direction, i.e., increase in clay content augmented the crystalline and decreased the amorphous phase, which agreed well with the homo-spectral correlation results. In practice, the application of PARAFAC kernel analysis was envisioned to provide opportunities to gain detailed information on sequences of species occurring under multiple perturbations.

4.4. Monitoring of ethanol production from immobilized yeast using homo- and hetero-covariance spectroscopy

As an example for process monitoring of biochemical processes, the conversion of glucose into alcohol by *Saccharomyces cerevisiae*, baker's or brewer's yeast, was monitored using low-field 1D ^{1}H NMR and Raman spectroscopy [65]. Monitoring of fermentation processes was described
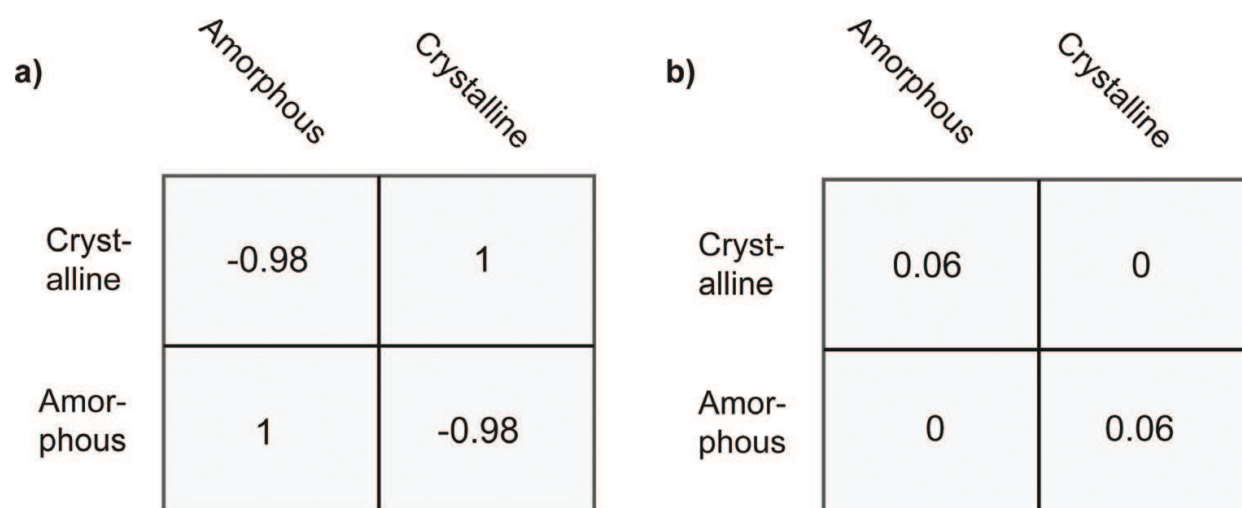

Figure 6. Representations of the q-synchronous kernel (a) and q-asynchronous kernel (b) matrices computed from the score matrix C of the clay weight-dependent 1D CP-MAS ^{13}C NMR spectra recorded at 100.56 MHz as used in the PARAFAC kernel analysis [34].

earlier, and NIR became the standard methodology [66, 67]. Later, attempts were made to use Raman spectroscopy [68]. Recently, hetero-spectral correlation NIR-IR spectroscopy was applied [69]. The fermentation described in the current report was conducted as a continuous process feeding glucose solution at a constant flow into a 2 L fermenter. Yeast immobilized within an alginate hydrocolloid converted the sugar to ethanol. The aqueous ethanolic solution was diverted at a constant flow. The flow rate was optimized such that during the residence time of a given volume, the glucose was fully converted into ethanol. On-line monitoring, i.e., through analysis of the ethanol signals and potential remainders of the glucose signals, was applied to control the efficiency of the process from the initial induction phase to the final stable production. After optimization, a sugar concentration of about 17% could be successfully transformed into ethanol.

Since no deuterated solvents were used, the series of 1D ^{1}H NMR spectra exhibited a dominant water signal and the typical ethanol resonances, cf. projections in **Figure 7**.

Homo- and hetero-covariance transformations were computed after spectral alignment and normalization to the water resonance at 4.8 ppm. The synchronous NMR spectrum displayed the expected positive intra-ethanol correlation at (3.8 ppm, 1.2 ppm). It exhibited further positive correlations between the signal at 4.8 ppm and the ethanol resonances at 1.2 and 3.8 ppm, suggesting that both signals increased or decreased in phase. As the spectra were normalized to the water resonance, the tentative change was traced back to changes in the linewidth of the water signal and should therefore not further be considered. Inspection of the asynchronous spectrum, cf. **Figure 7**, showed no intramolecular correlations at 3.8 and 1.2 ppm as would be expected, since the ethanol signals would change in phase. Yet, correlations between the signal at 4.8 ppm and the ethanol resonances were observed. The sign of the correlation suggested that water or an underlying component would grow before ethanol
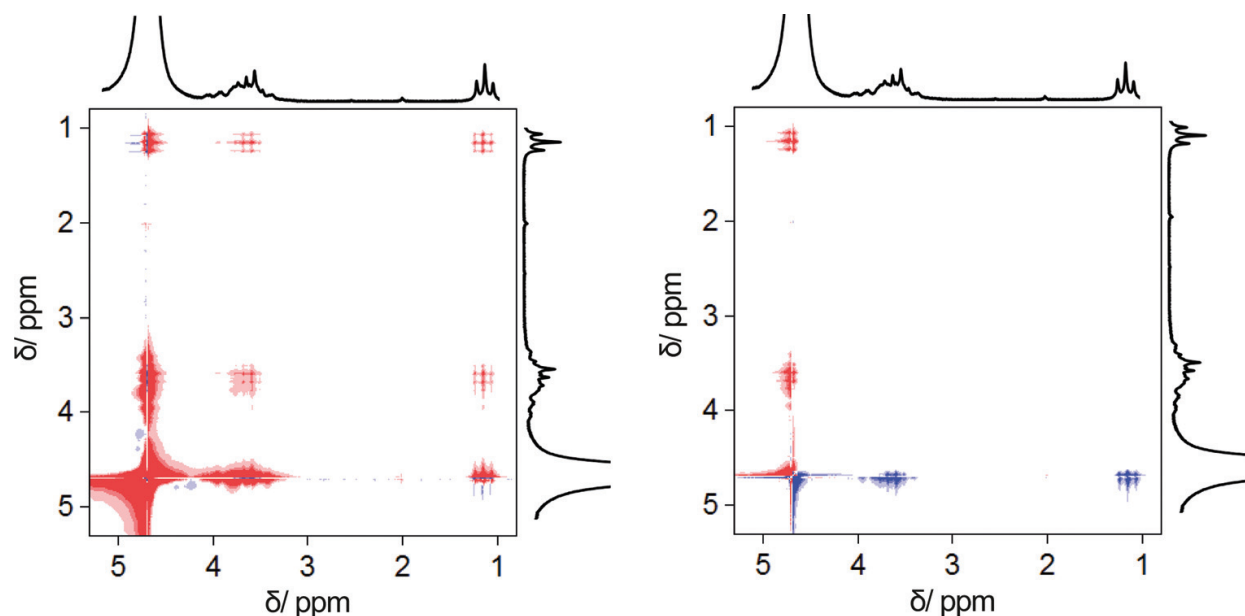

Figure 7. Synchronous (left) and asynchronous (right) 2D NMR homo-correlation spectra of ethanol production by immobilized yeast using on-line 1D ^{1}H NMR spectroscopy (82 MHz, T = 36°C).

increased. Since change on the water resonance was traced back to linewidth variations, no conclusion with respect to the sequence of change should be drawn. Taking into account the earlier observation by Kirwan et al. and Sasic with respect to changes in linewidth and spectral alignment, the described preprocessing procedures were found difficult to apply to low-field spectra with relatively poor resolution and signals with strongly differing linewidths.

In contrast, the hetero-covariance NMR-Raman spectrum proved very useful for the quick analysis and assignment of the signals in the Raman spectrum, cf. **Figure 8**.

Only the band at 1360 cm^{-1} showed a negative correlation with the NMR resonances of ethanol, thus identifying this band as educt related. All other Raman bands were found in phase with the ethanol NMR signals and could thus serve for product monitoring. The hetero-correlation spectrum was hence able to readily visualize that nearly all Raman bands at least predominantly originated from ethanol, but in contrast to low-field NMR signals provided an educt signal, which appeared only as a shoulder in the corresponding 1D Raman spectrum.

4.5. Reaction monitoring of a Knoevenagel condensation in a microreaction system

A Knoevenagel condensation reaction was conducted in a microreaction system, cf. **Figure 2** [70]. Neat malonic acid diethylester and 2-propanal were flowed through the microreactor at a
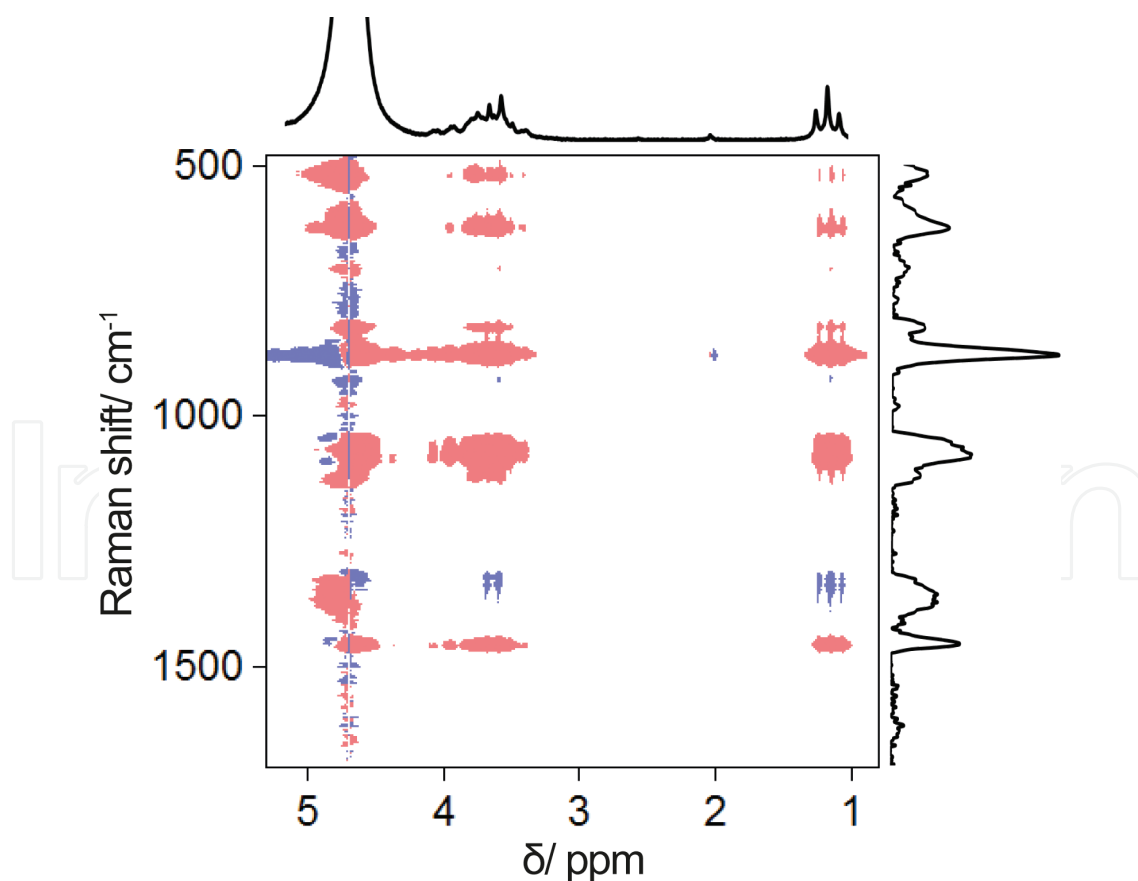

Figure 8. 2D NMR-Raman hetero-correlation spectra of ethanol production by immobilized yeast using on-line 1D ^{1}H NMR spectroscopy (82 MHz, T = 36°C) and in-line Raman spectroscopy (laser wavelength 785 nm).

temperature of 82°C. Butylidene malonic acid diethylester and water were obtained as products. The solution was re-circulated for 1200 min and monitored using on-line low-field benchtop 1D ^{1}H NMR (82 MHz), in-line NIR, and in-line Raman spectroscopy (laser excitation wavelength 785 nm). Despite the relatively poor resolution of the low-field instrument, the series of 1D ^{1}H NMR spectra showed well-resolved signals for each educt and product, cf. **Figure 9**. Therefore, signals could be integrated and concentration-time plots were established.

The covariance transformation to synchronous and asynchronous homo-spectral correlation maps helped quickly visualize the interdependence of the signals, cf. **Figure 10**. The assignment of educt and product signals was in agreement with correlation crosspeaks and their signs. The signals were attributed as 3.2 ppm for malonic acid diethylester, 6.8 ppm for the product butylidene malonic diethylester, and 9.5 ppm for 2-propanal. Since the intensity of the autopeaks in the homo-covariance map reflects the amount of change, peaks appeared at strongly different intensity levels such that representations of the spectra should be prepared using different thresholds with emphasis on either strong or weak signals. Nevertheless, the sign of the crosspeaks was found in accordance with the expectancy values. With respect to the
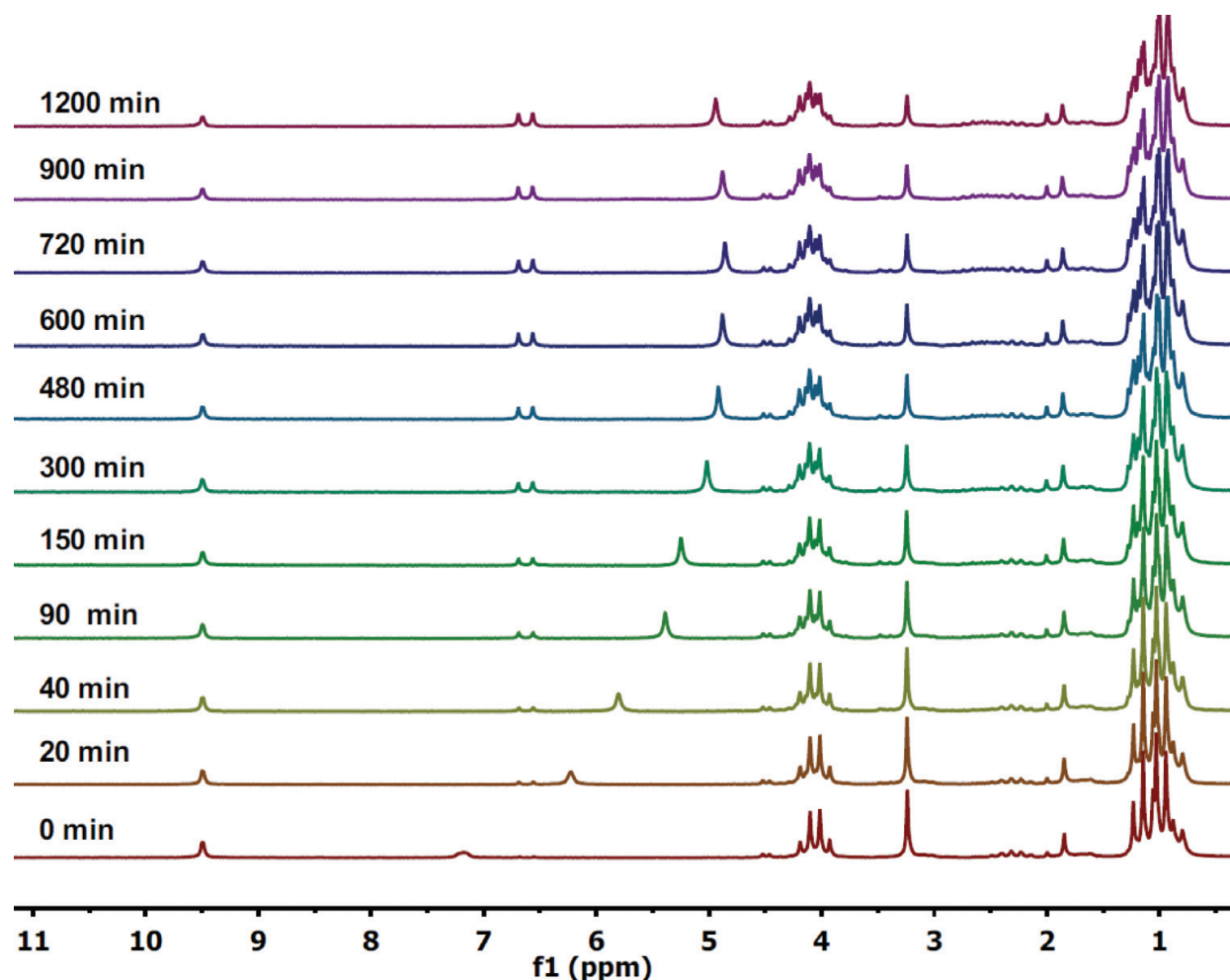

Figure 9. 1D ^{1}H NMR spectra (82 MHz, T = 36°C) recorded for 1200 min during on-line monitoring of a Knoevenagel condensation of neat malonic acid diethylester and 2-propanal yielding butylidene malonic acid diethylester conducted in a microreaction system presented in Figure 2.
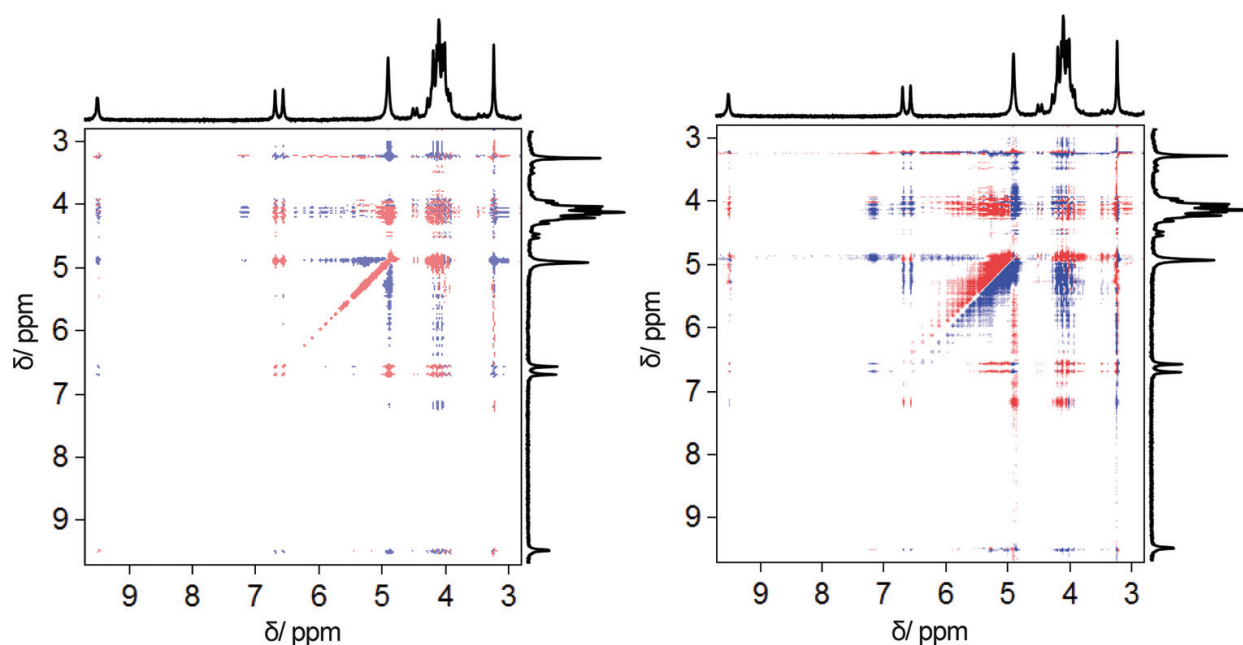
Figure 10. Synchronous (left) and asynchronous (right) 2D NMR correlation spectra of a Knoevenagel condensation of neat malonic acid diethylester and 2-propanal yielding butylidene malonic acid diethylester conducted in a microreaction system and monitored during 1200 min at a reaction temperature of 82°C using on-line 1D ^{1}H NMR (82 MHz, T = 36°C).

asynchronous map, the positive crosspeak at 9.5 and 6.8 ppm was seen indicative for the aldehyde reaction preceding the final product formation, i.e., the formation of the double bond.

Although the interpretation of the 1D ^{1}H NMR spectra was readily achieved, the use of in-line applicable techniques such as Raman and NIR spectroscopy was considered preferable from a process analytical perspective. This required the interpretation of the vibrational spectra. The increasing intensity of the Raman band at 1600 cm^{-1}, which originated from the carbon-carbon double bond vibration, was to some extent obvious in the series of 1D Raman spectra recorded. Further attribution of bands useful for reaction component monitoring was not readily achieved. To this purpose, hetero-correlation maps were computed from NMR and Raman spectra as well as from NMR and NIR, shown in **Figure 11**. Preprocessing of all spectra with respect to baseline correction, alignment, normalization, and data reduction or binning was found of utmost importance. The NMR signal assignment was readily transferred to the bands at 1600 and 800 cm^{-1} through correlations. The band at 800 cm^{-1} exhibited negative correlations to the product chemical shift and was hence found due to one of the educts. On inspection of the aldehyde resonance at 9.5 ppm, positive signs were found, which would be expected for a correlation between educts. The band at 1450 cm^{-1}, which was assigned to a methylene group bending vibration, showed only weak correlations. One of them correlated that band to the resonance at 3.2 ppm, indicating an educt-educt relationship. Analyzing the NIR-NMR hetero-covariance spectra, the enhancing power of NMR spectroscopy becomes even more evident. While NIR provides very broad bands that are due to either C-H or O-H overtone or combination frequencies and thus seemingly non-specific, the well-resolved signals of NMR spectroscopy assist in finding regions that can be attributed to educts or products and thus used for
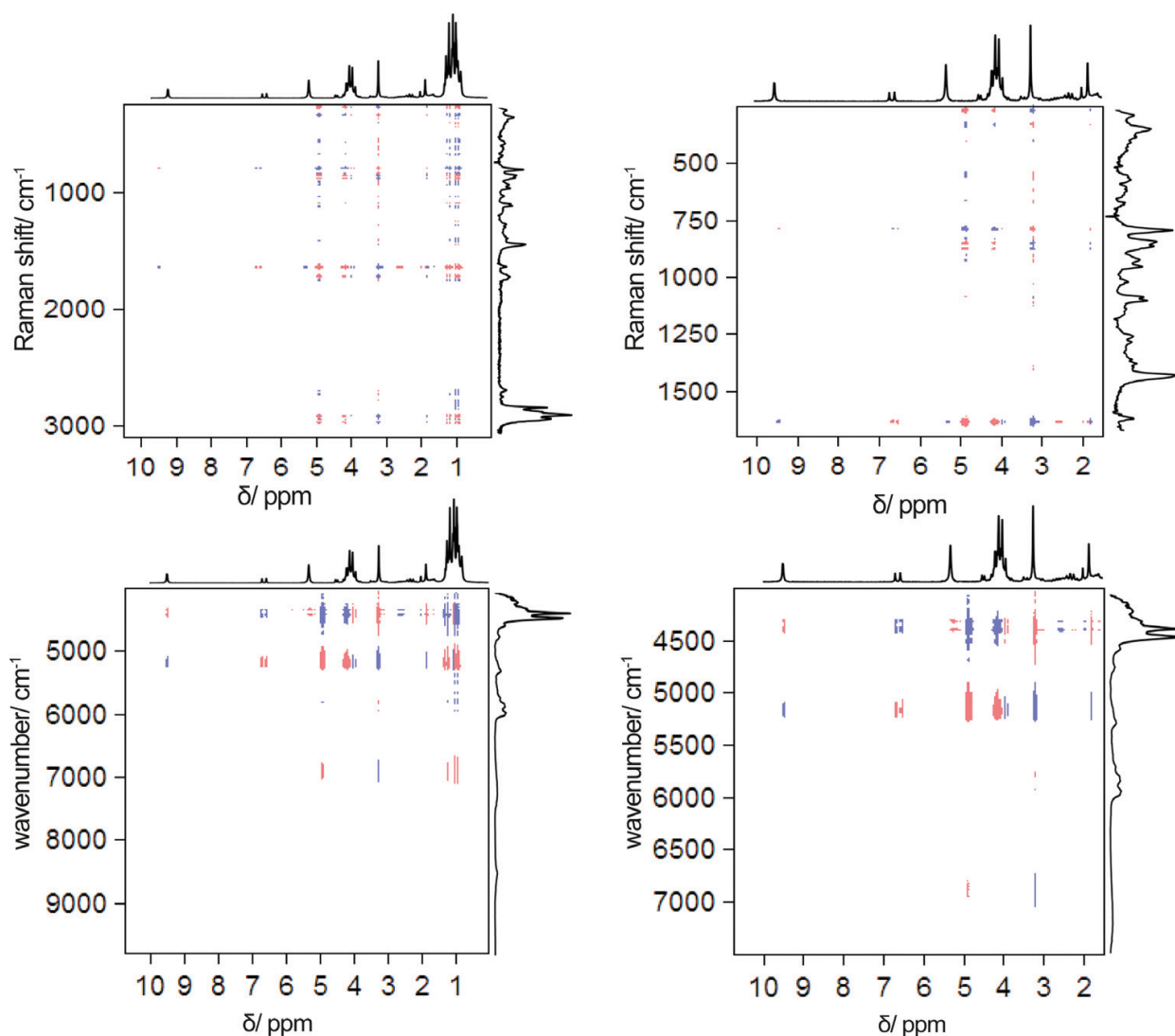
Figure 11. Synchronous Raman-NMR (top row) and NIR-NMR (bottom row) hetero-correlation spectra of a Knoevenagel condensation of neat malonic acid diethylester and 2-propanal yielding butylidene malonic acid diethylester conducted in a microreaction system and monitored during 1200 min at a reaction temperature of 82°C using on-line 1D ^{1}H NMR (82 MHz, T = 36°C), in-line NIR and in-line Raman spectroscopy (laser wavelength of 785 nm); full spectrum (left) and enlarged region (right), 1D spectra recorded at 1200 min are shown top and right of the correlation map.

reaction monitoring. The NIR-NMR correlation signals in **Figure 11**, bottom row, indicate that the O-H resonance around 7000 cm^{-1} stemmed from product water, while that around 5200 cm^{-1} was due to an educt C-H combination frequency. Thus, two potential monitoring frequency ranges could be identified.

Based on the thus identified and attributed signals, intensity-time plots and hence concentration-time curves could be extracted from the series of one-dimensional NIR spectra. This allowed the comparison of reaction monitoring by three different spectroscopic techniques, NIR, Raman, and NMR. The results were found in rather good agreement with each other. The concentration-time curves could be computed using chemical kinetic models from which reaction rate constants and half-lives were obtained. The reaction was found to follow first- or pseudo first-order reaction

kinetics. It was expected that the knowledge of reaction parameters could later be transformed into automatic process control [70].

5. Conclusion

Covariance NMR has become a valuable tool in the ensemble of NMR methodologies. Generalized covariance was often performed with techniques other than NMR to profit from synchronous and asynchronous correlation maps. The synchronous map as a substitute to or along with the traditional Fourier transformed spectrum was nevertheless employed quite frequently in NMR. Hetero-spectroscopic covariance was used to concatenate NMR and mass spectrometry, NIR, and Raman data allowing combining the information of two techniques. Resolution improvement was reported an advantage of both the homo- and hetero-covariance processing, since information could be transferred from the well-resolved NMR domain into the less obvious to interpret vibrational domains. Here, the synchronous spectrum helped to increase resolution and assign signals to either the same or different species. As had been reported for vibrational spectroscopy, homo-covariance transformation also gives rise to two-dimensional data when only series of 1D NMR spectra are available, e.g., due to the application of low-field NMR instruments. Although the asynchronous map provides information on the sequential occurrence of signals, it has been relatively rarely exploited for NMR purposes. In a more recent study, Noda showed that more sophisticated mathematical processing was needed to derive the order of three or more species within a chemical reaction. When the asynchronous spectra were computed and analyzed, the sequential attribution feature proved very useful for PAT applications, such as in fermentation or reaction monitoring. Examples of wine fermentation, ethanol production using immobilized yeast, and monitoring of a radical polymerization and a Knoevenagel condensation in a microreaction system with a low-field NMR instrument were discussed. For quantitation of signal intensity changes and conclusions therefrom, the PARAFAC kernel analysis applied to polylactic acid nanocomposites with various clay content and at varied temperatures was summarized.

The opportunities of homo- and hetero-covariance spectroscopy in the field of NMR combined with other spectroscopic and spectrometric techniques are numerous. Still, new mathematical extensions continue to be devised. The authors therefore expect that with commercial software becoming more available for non-developing users, the reports on applications of homo- and hetero-covariance spectroscopy yielding synchronous and asynchronous spectra to chemical problems will steadily grow.

Acknowledgements

Author details

Martin Jaeger* and Robin Legner

*Address all correspondence to: martin.jaeger@hs-niederrhein.de

Department of Chemistry, Instrumental Analytical Chemistry and ILOC Institute for Coatings and Surface Chemistry, Niederrhein University, Krefeld, Germany

References

[1] Snyder DA, Bruschweiler R, Williams T, Martin G, Rovnyak D. Multi-dimensional spin correlations by covariance NMR. In: Modern NMR Approaches to the Structure Elucidation of Natural Products: Volume 1: Instrumentation and Software. The Royal Society of Chemistry. Cambridge, UK, 2016; pp. 244–258. DOI: 10.1039/9781849735186-00244

[2] Snyder DA, Bruschweiler R, Brüschweiler R, et al, Morris GE, Emsley JW. Multidimensional correlation spectroscopy by covariance NMR. In: Multidimensional NMR Methods for the Solution State. Chichester, UK: John Wiley & Sons Ltd, 2009; pp. 97–105. DOI: 10.1002/9780470034590.emrstm1098

[3] Jaeger M, Aspers RLEG. Covariance NMR and small molecule applications. Annual Reports on NMR Spectroscopy. 2014;**83**:271–349. DOI: 10.1016/B978-0-12-800183-7.00005-8

[4] Jaeger M, Aspers RLEG, Voigt M. Covariance NMR. In: Lindon JC, Tranter GE, Koppenaal DW (eds.) The Encyclopedia of Spectroscopy and Spectrometry, 3rd edition, 2017;**1**:396–400. Oxford: Academic Press. DOI: 10.1016/B978-0-12-409547-2.12106-7

[5] Park Y, Noda I, Jung YM. Novel developments and applications of two-dimensional correlation spectroscopy. Journal of Molecular Structure. 2016;**1124**:11–28. DOI: http://dx.doi.org/10.1016/j.molstruc.2016.01.028

[6] Noda I. Frontiers of two-dimensional correlation spectroscopy. Part 1. New concepts and noteworthy developments. Journal of Molecular Structure. 2014;**1069**:3–22. DOI: http://dx.doi.org/10.1016/j.molstruc.2014.01.025

[7] Noda I. Frontiers of two-dimensional correlation spectroscopy. Part 2. Perturbation methods, fields of applications, and types of analytical probes. Journal of Molecular Structure. 2014;**1069**:23–49. DOI: 10.1016/j.molstruc.2014.01.016

[8] Blinov KA, Larin NI, Williams AJ, et al. Unsymmetrical covariance processing of COSY or TOCSY and HSQC NMR data to obtain the equivalent of HSQC-COSY or HSQC-TOCSY spectra. Journal of Heterocyclic Chemistry. 2006;**43**:163–166. DOI: 10.1002/jhet.5570430124

[9] Noda I. Two-dimensional infrared spectroscopy. Journal of the American Chemical Society. 1989;**111**:8116–8118. DOI: 10.1021/ja00203a008

[10] Frasinski LJ, Codling K, Hatherly PA. Covariance mapping: A correlation method applied to multiphoton multiple ionization. Science. 1989;**246**:1029–1031. DOI: 10.1126/science.246.4933.1029

[11] Noda I. Two-dimensional infrared (2D IR) spectroscopy: Theory and applications. Applied Spectroscopy. 1990;**44**:550–561. DOI: 10.1366/0003702904087398

[12] Noda I. Generalized two-dimensional correlation method applicable to infrared, raman, and other types of spectroscopy. Applied Spectroscopy. 1993;**47**:1329–1336. DOI: 10.1366/0003702934067694

[13] Noda I, Dowrey AE, Marcott C, et al. Generalized two-dimensional correlation spectroscopy. Applied Spectroscopy. 2000;**54**:236A-248A. DOI: 10.1366/0003702001950454

[14] Eads CD, Noda I. Generalized correlation NMR spectroscopy. Journal of the American Chemical Society. 2002;**124**:1111–1118. DOI: 10.1021/ja011819v

[15] Noda I. Determination of two-dimensional correlation spectra using the Hilbert transform. Applied Spectroscopy. 2000;**54**:994–999. DOI: 10.1366/0003702001950472

[16] Bruschweiler R. Theory of covariance nuclear magnetic resonance spectroscopy. The Journal of Chemical Physics. 2004;**121**:409–414. DOI: 10.1063/1.1755652

[17] Ernst RR, Bodenhausen G, Wokaun A. Principles of Nuclear Magnetic Resonance in One and Two Dimensions. Oxford: Clarendon Press; 1990. Available from: http://books.google.de/books?id=4bohtceju9kC

[18] Bax A. Two-Dimensional Nuclear Magnetic Resonance in Liquids. Dordrecht, Holland: D. Reidel Publishing Company; 1982

[19] Martin GE, Irish PA, Hilton BD, et al. Utilizing unsymmetrical indirect covariance processing to define 15N-13C connectivity networks. Magnetic Resonance in Chemistry. 2007;**45**:624–627. DOI: 10.1002/mrc.2029

[20] Martin GE, Hilton BD, Irish PA, et al. Application of unsymmetrical indirect covariance NMR methods to the computation of the 13C.tautm.15N HMBC-IMPEACH correlation spectra. Magnetic Resonance in Chemistry. 2007;**45**:883–888. DOI: 10.1002/mrc.2064

[21] Martin GE, Hilton BD, Blinov KA, et al. Using indirect covariance spectra to identify artifact responses in unsymmetrical indirect covariance calculated spectra. Magnetic Resonance in Chemistry. 2008;**46**:138–143. DOI: 10.1002/mrc.2141

[22] Crockford DJ, Holmes E, Lindon JC, et al. Statistical heterospectroscopy, an approach to the integrated analysis of NMR and UPLC-MS data sets: Application in metabonomic toxicology studies. Analytical Chemistry. 2006;**78**:363–371. DOI: 10.1021/ac051444m

[23] Bruschweiler R, Zhang F. Covariance nuclear magnetic resonance spectroscopy. The Journal of Chemical Physics. 2004;**120**:5253–5260. DOI: 10.1063/1.1647054

[24] Hu B-W, Zhou P, Noda I, et al. An NMR approach applicable to biomolecular structure characterization. Analytical Chemistry. 2005;**77**:7534–7538. DOI: 10.1021/ac051061o

[25] Noda I. Two-dimensional codistribution spectroscopy to determine the sequential order of distributed presence of species. Journal of Molecular Structure. 2014;**1069**:50–59. DOI: 10.1016/j.molstruc.2014.01.024

[26] Martin GE. Posaconazole: Application of HSQC-ADEQUATE from general indirect covariance processing. Journal of Heterocyclic Chemistry. 2012;**49**:716–720. DOI: 10.1002/jhet.892

[27] Aspers RLEG, Geutjes PETJ, Honing M, et al. Using indirect covariance processing for structure elucidation of small molecules in cases of spectral crowding. Magnetic Resonance in Chemistry. 2011;**49**:425–436. DOI 10.1002/mrc.2766

[28] Zhang F-L, Bruschweiler-Li L, Bruschweiler R. Simultaneous de novo identification of molecules in chemical mixtures by doubly indirect covariance NMR spectroscopy. Journal of the American Chemical Society. 2010;**132**:16922–16927. DOI: 10.1021/ja106781r

[29] Bingol K, Salinas RK, Brueschweiler R. Higher-rank correlation NMR spectra with spectral moment filtering. The Journal of Physical Chemistry Letters. 2010;**1**:1086–1089. DOI: 10.1021/jz100264g

[30] Lindon JC, Nicholson JK. Spectroscopic and statistical techniques for information recovery in metabonomics and metabolomics. Annual Review of Analytical Chemistry. 2008;**1**:45–69. DOI: 10.1146/annurev.anchem.1.031207.113026

[31] Robinette SL, Zhang F, Bruschweiler-Li L, et al. Web server based complex mixture analysis by NMR. Analytical Chemistry (Washington, DC, USA). 2008;**80**:3606–3611. DOI: 10.1021/ac702530t

[32] Robinette SL, Lindon JC, Nicholson JK. Statistical spectroscopic tools for biomarker discovery and systems medicine. Analytical Chemistry. 2013;**85**:5297–5303. DOI: 10.1021/ac4007254

[33] Noda I. Recent developments in two-dimensional (2D) correlation spectroscopy. Chinese Chemical Letters. 2015;**26**:167–172. DOI: 10.1016/j.cclet.2014.10.006

[34] Shinzawa H, Nishida M, Kanematsu W, et al. Parallel factor (PARAFAC) kernel analysis of temperature- and composition-dependent NMR spectra of poly(lactic acid) nanocomposites. Analyst. 2012;**137**:1913–1921. DOI: 10.1039/C2AN16019F

[35] Tomasi G, Bro R. A comparison of algorithms for fitting the PARAFAC model. Computational Statistics & Data Analysis. 2006;**50**:1700–1734. DOI: http://dx.doi.org/10.1016/j.csda.2004.11.013

[36] Smilde A, Bro R, Geladi P. Three-Way component and regression models. In: Multi-Way Analysis with Applications in the Chemical Sciences. John Wiley & Sons, Ltd, Chichester, UK, 2004; pp. 57–87. DOI: 10.1002/0470012110.ch4

[37] Qi J, Li H, Huang K, et al. Orthogonal sample design scheme for two-dimensional synchronous spectroscopy and its application in probing intermolecular interactions. Applied Spectroscopy. 2007;**61**:1359–1365. DOI: 10.1366/000370207783291993

[38] Qi J, Huang K, Gao X, et al. Orthogonal sample design scheme for two-dimensional synchronous spectroscopy: Application in probing lanthanide ions interactions with organic ligands in solution mixtures. Journal of Molecular Structure. 2008;**883-884**:116–123. DOI: 10.1016/j.molstruc.2008.01.036

[39] Liu Y, Zhang C, Liu S, et al. Modified orthogonal sample design scheme to probe intermolecular interactions. Journal of Molecular Structure. 2008;**883-884**:124–128. DOI: 10.1016/j.molstruc.2007.12.025

[40] Shinzawa H, Morita S-I, Awa K, et al. Multiple perturbation two-dimensional correlation analysis of cellulose by attenuated total reflection infrared spectroscopy. Applied Spectroscopy. 2009;**63**:501–506. DOI: 10.1366/000370209788346977

[41] Shinzawa H, Hashimoto K, Sato H, et al. Multiple-perturbation two-dimensional (2D) correlation analysis for spectroscopic imaging data. Journal of Molecular Structure. 2014;**1069**:176–182. DOI: 10.1016/j.molstruc.2014.02.013

[42] Noda I. Two-dimensional correlation spectroscopy—Biannual survey 2007-2009. Journal of Molecular Structure. 2010;**974**:3–24. DOI: 10.1016/j.molstruc.2010.01.069

[43] FDA. Guidance for industry PAT: A framework for innovative pharmaceutical development, manufacuring, and quality assurance. FDA Off Doc. 2004;**16**. DOI: http://www.fda.gov/CDER/guidance/6419fnl.pdf

[44] (a) EMEA PAT Team, Reflection Paper, Chemical, pharmaceutical and biological information to be included in dossiers when Process Analytical Technology (PAT) is employed. EMEA/INS/277260/2005, March 2006. (b) EMEA Note for guidance on analytical development, EMEA/CHMP/ICH/167068/2004

[45] Kessler RW, editor. Prozessanalalytik: Strategien und Fallbeispiele aus der industriellen Praxis. Weinheim: Wiley-VCH; 2006

[46] Bakeev KA, editor. Process Analytical Technology. Spectroscopic Tools and Implementation Strategies for the Chemical and Pharmaceutical Industries. 2nd ed. Chichester: John Wiley & Sons, Ltd; 2010

[47] Jähnisch K, Hessel V, Löwe H, et al. Chemistry in microstructured reactors. Angewandte Chemie International Edition. 2004;**43**:406–446. DOI: 10.1002/anie.200300577

[48] Bogdan AR, Poe SL, Kubis DC, et al. The continuous-flow synthesis of ibuprofen. Angewandte Chemie. 2009;**121**:8699–8702. DOI: 10.1002/ange.200903055

[49] Ehrfeld W, Hessel V, Löwe H. Microreactors—New technology for modern chemistry. Organic Process Research & Development. 2001;**5**:89–89. DOI: 10.1021/op000071i

[50] Zalesskiy SS, Danieli E, Blümich B, et al. Miniaturization of NMR systems: Desktop spectrometers, microcoil spectroscopy, and 'NMR on a Chip' for chemistry, biochemistry, and industry. Chemical Reviews. 2014;**114**:5641–5694. DOI: 10.1021/cr400063g

[51] Danieli E, Perlo J, Duchateau ALL, et al. On-line monitoring of chemical reactions by using Bench-Top nuclear magnetic resonance spectroscopy. ChemPhysChem. 2014;**15**:3060–3066. DOI: 10.1002/cphc.201402049

[52] McGill CA, Nordon A, Littlejohn D. Comparison of in-line NIR, Raman and UV-visible spectrometries, and at-line NMR spectrometry for the monitoring of an esterification reaction. Analyst. 2002;**127**:287–292. DOI: 10.1039/B106889J

[53] Maiwald M, Fischer HH, Kim YK, et al. Quantitative high-resolution on-line NMR spectroscopy in reaction and process monitoring. Journal of Magnetic Resonance. 2004;**166**:135–146. DOI: 10.1016/j.jmr.2003.09.003

[54] Li Y, Hu B, Chen Q, et al. Comparison of various sampling schemes and accumulation profiles in covariance spectroscopy with exponentially decaying 2D signals. Analyst. 2013;**138**:2411–2419. DOI: 10.1039/C3AN36375A

[55] Lafon O, Hu B, Amoureux J-P, et al. Fast and high-resolution stereochemical analysis by nonuniform sampling and vovariance processing of anisotropic natural abundance 2D 2H NMR datasets. Chemistry—A European Journal. 2011;**17**:6716–6724. S6716/1–S6716/6. DOI: 10.1002/chem.201100461

[56] Chen Y, Zhang F, Bermel W, et al. Enhanced covariance spectroscopy from minimal datasets. Journal of the American Chemical Society. 2006;**128**:15564–15565. DOI: 10.1021/ja065522e

[57] Li Y, Wang Q, Zhang Z, et al. Covariance spectroscopy with a non-uniform and consecutive acquisition scheme for signal enhancement of the NMR experiments. Journal of Magnetic Resonance. 2012;**217**:106–111. DOI: 10.1016/j.jmr.2012.02.016

[58] Takeda K, Kusakabe Y, Noda Y, et al. Homo- and heteronuclear two-dimensional covariance solid-state NMR spectroscopy with a dual-receiver system. Physical Chemistry Chemical Physics. 2012;**14**:9715–9721. DOI: 10.1039/c2cp41191a

[59] Garcia H, Barros AS, Gonçalves C, et al. Characterization of dextrin hydrogels by FTIR spectroscopy and solid state NMR spectroscopy. European Polymer Journal. 2008;**44**:2318–2329. DOI: 10.1016/j.eurpolymj.2008.05.013

[60] Robinette SL, Bruschweiler R, Schroeder FC, et al. NMR in metabolomics and natural products research: Two sides of the same coin. Accounts of Chemical Research. 2012;**45**:288–297. DOI: 10.1021/ar2001606

[61] Kirwan GM, Clark S, Barnett NW, et al. Generalised 2D-correlation NMR analysis of a wine fermentation. Analytica Chimica Acta. 2008;**629**:128–135. DOI: 10.1016/j.aca.2008.09.046

[62] Sasic S. Two-dimensional correlation analysis of nuclear magnetic resonance metabonomics data. Applied Spectroscopy. 2008;**62**:840–846. DOI: 10.1366/000370208785284439

[63] Kirwan GM, Adams MJ. Peak width issues with generalised 2D correlation NMR spectroscopy. Journal of Molecular Structure. 2008;**892**:225–230. DOI: 10.1016/j.molstruc.2008.05.031

[64] Ryu SR, Bae WM, Hong WJ, et al. Characterization of chain transfer reaction during radical polymerization of silver nanocomposite polyvinylpyrrolidone by using 2D hetero-spectral IR/NMR correlation spectroscopy. Vibrational Spectroscopy. 2012;**60**:168–172. DOI: 10.1016/j.vibspec.2011.12.009

[65] Legner R, Wirtz A, Tiedt M, et al. On-line monitoring of ethanol fermentation using homo and hetero covariance low-field NMR, Raman and NIR spectroscopy. Prep

[66] Cavinato AG, Mayes DM, Ge Z, et al. Noninvasive method for monitoring ethanol in fermentation processes using fiber-optic near-infrared spectroscopy. Analytical Chemistry. 1990;**62**:1977–1982. DOI: 10.1021/ac00217a015

[67] Blanco M, Peinado AC, Mas J. Analytical monitoring of alcoholic fermentation using NIR spectroscopy. Biotechnology and Bioengineering. 2004;**88**:536–542. DOI: 10.1002/bit.20214

[68] Burikov S, Dolenko T, Patsaeva S, et al. Raman and IR spectroscopy research on hydrogen bonding in water–ethanol systems. Molecular Physics. 2010;**108**:2427–2436. DOI: 10.1080/00268976.2010.516277

[69] Nishii T, Genkawa T, Watari M, et al. Selection of the NIR region for a regression model of the ethanol concentration in fermentation process by an online NIR and Mid-IR Dual-Region spectrometer and 2D heterospectral correlation spectroscopy. Analytical Sciences. 2012;**28**:1165–1170. DOI: 10.2116/analsci.28.1165

[70] Legner R, Haefner S, Voigt M, et al. Micro process analytical technology. GIT Lab J. 2016;**3-4**:38–40. Available from: http://www.laboratory-journal.com/science/chemistry-physics/microprocess-analytical-technology